

# Analyzing Dynamic Behavior of Geosynthetic-Reinforced Soil Retaining Walls

Hoe I. Ling, M.ASCE<sup>1</sup>; Huabei Liu<sup>2</sup>; Victor N. Kaliakin, M.ASCE<sup>3</sup>; and Dov Leshchinsky, M.ASCE<sup>4</sup>

**Abstract:** An advanced generalized plasticity soil model and bounding surface geosynthetic model, in conjunction with a dynamic finite element procedure, are used to analyze the behavior of geosynthetic-reinforced soil retaining walls. The construction behavior of a full-scale wall is first analyzed followed by a series of five shaking table tests conducted in a centrifuge. The parameters for the sandy backfill soils are calibrated through the results of monotonic and cyclic triaxial tests. The wall facing deformations, strains in the geogrid reinforcement layers, lateral earth pressures acting at the facing blocks, and vertical stresses at the foundation are presented. In the centrifugal shaking table tests, the response of the walls subject to 20 cycles of sinusoidal wave having a frequency of 2 Hz and of acceleration amplitude of 0.2g are compared with the results of analysis. The acceleration in the backfill, strain in the geogrid layers, and facing deformation are computed and compared to the test results. The results of analysis for both static and dynamic tests compared reasonably well with the experimental results.

**DOI:** 10.1061/(ASCE)0733-9399(2004)130:8(911)

**CE Database subject headings:** Retaining walls; Soil structures; Geosynthetics; Plasticity; Finite elements.

## Introduction

The finite element method has been used successfully in simulating the behavior of geosynthetic-reinforced soil retaining walls under static loading conditions (e.g., Collin 1986; Kaliakin and Xi 1992; Kapurapu and Bathurst 1995; Ling et al. 1995, 2000; Rowe and Ho 1997), but very limited studies have been reported for the simulation of the dynamic behavior (Segrestin and Bastick 1988; Yogendrakumar et al. 1992; Cai and Bathurst 1995; Helwany et al. 2001) and these were all equivalent linear analyses. The simulation of dynamic soil structure response is complicated by the highly nonlinear behavior of soil and numerical algorithms. Soil stress–deformation behavior is affected by the confining stress as well as the initial density. Generally, dense sand dilates upon shearing whereas loose sand contracts, but the confining pressure affects deformation characteristics at the different states. For nonsaturated soils, although liquefaction is not a concern, the stress–strain response exhibits hysteresis and hardening behavior under repeated loadings. Many constitutive models have been

proposed to simulate the inelastic soil behavior, but the number of soil models relevant for cyclic loading of sand is still very limited.

The literature on the dynamic behavior of reinforced soil walls is concentrated on postearthquake investigations (e.g., Tatsuoka et al. 1998; Ling et al. 2001a), which in most cases, lacked proper characterization of soil properties. The stress conditions and wall deformation before the earthquake, as well as the input acceleration, were not readily known. Detailed knowledge of the response of a reinforced soil wall during an earthquake, including soil acceleration and deformation, strains in the reinforcements, etc., are required for an adequate understanding of the dynamic behavior.

Laboratory model tests are very instrumental in studying the behavior of reinforced soil walls under controlled conditions. However, most shaking table tests are conducted using reduced scale models in a 1g field ( $g$ : gravity) (e.g., Bathurst et al. 2001; Koseki et al. 2003) that are possibly subject to scale effects due to the influence of stress levels and the lack of reasonable scaling techniques. On the other hand, the centrifugal modeling technique has proved extremely useful in simulating the stress level using reduced scale models. According to the scaling rules, the stress–strain behavior of the centrifuge model, which is of dimension  $n$  times smaller than the prototype, is preserved if the acceleration is increased by  $n$  times the gravity. For dynamic events in a centrifuge, the frequency has to be increased by  $n$  times whereas the time is reduced by  $n$  times. Applications of centrifugal modeling techniques to reinforced soil retaining walls and slopes have been reported by several researchers but these tests were mostly limited to static conditions (e.g., Bolton et al. 1979; Jaber et al. 1990; Porbaha and Goodings 1996; Zornberg et al. 1998). The centrifugal shaking table tests of Kutter et al. (1990) and Sakaguchi (1996) are limited examples. The tests by Kutter et al. (1990) were well planned but metallic reinforcements were used. Sakaguchi (1996) conducted tests by varying the variables such as the reinforcement spacing and length.

Under the U.S.—Japan collaborative research effort, a series of five shaking table tests were conducted using the centrifuge

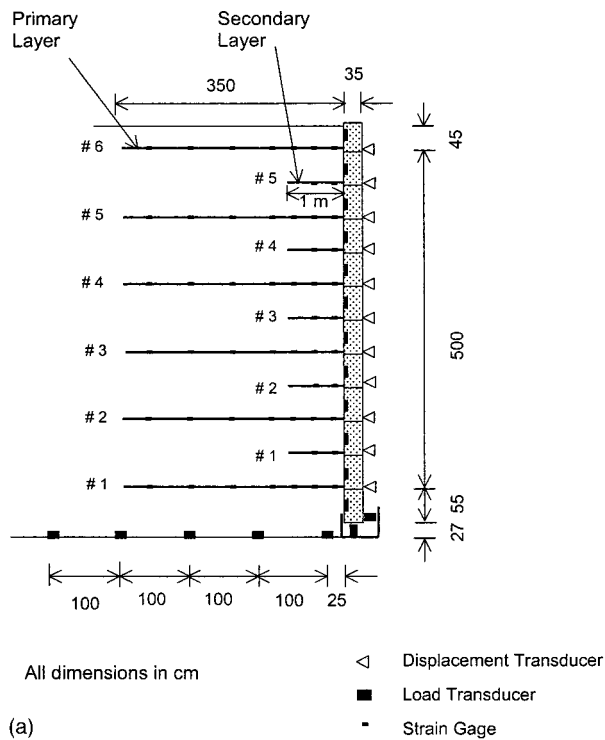
<sup>1</sup>Associate Professor, Dept. of Civil Engineering and Engineering Mechanics, Columbia Univ., 500 West 120th St., New York, NY 10027. E-mail: ling@civil.columbia.edu

<sup>2</sup>Graduate Research Assistant, Dept. of Civil Engineering and Engineering Mechanics, Columbia Univ., New York, NY 10027.

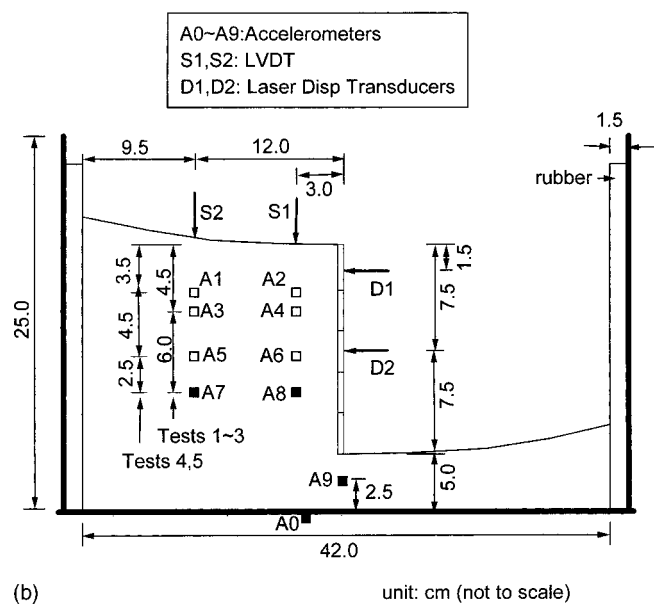
<sup>3</sup>Associate Professor, Dept. of Civil and Environmental Engineering, Univ. of Delaware, Newark, DE 19716.

<sup>4</sup>Professor, Dept. of Civil and Environmental Engineering, Univ. of Delaware, Newark, DE 19716.

Note. Associate Editor: Eric N. Landis. Discussion open until January 1, 2005. Separate discussions must be submitted for individual papers. To extend the closing date by one month, a written request must be filed with the ASCE Managing Editor. The manuscript for this paper was submitted for review and possible publication on March 31, 2003; approved on January 12, 2004. This paper is part of the *Journal of Engineering Mechanics*, Vol. 130, No. 8, August 1, 2004. ©ASCE, ISSN 0733-9399/2004/8-911–920/\$18.00.



(a)



(b)

**Fig. 1.** (a) Public Works Research Institute Wall and (b) centrifuge model

facility at the Tokyo Institute of Technology shortly after the 1995 Kobe earthquake. The results of centrifuge model tests have been reported by Takahashi et al. (1999) and Takemura and Takahashi (2003) and this paper is concentrated on the numerical simulation of their test results. The finite element procedures together with an advanced soil constitutive model are used. The validity of numerical procedures in simulating the behavior of a segmental block reinforced soil wall is first verified against a full-scale test wall constructed at the Public Works Research Institute (PWRI), Japan. The dynamic centrifuge models are then briefly described followed by details of analysis. The finite element results are compared with the experimental results and discussed.

**Table 1.** Reinforcement Layout for Centrifuge Tests

Test No.	Length	Spacing
1	1.0H	0.2H
2	0.8H	0.2H
3	0.6H	0.2H
4	0.8H	0.1H
5	0.6H	0.1H

**Physical Models**

A brief description of the PWRI Wall is given followed by the dynamic centrifuge models. It has to be noted that the centrifuge models were not the physical models for simulating the PWRI Wall. They are two independent sets of physical models used in this study for validating numerical tools.

**Public Works Research Institute Wall**

This well documented case history was undertaken to monitor the construction behavior of a reinforced segmental-block wall. Basic information of the PWRI Wall has been reported by Tajiri et al. (1996). Additional details, such as the wall configuration, soil, and reinforcement properties, as well as interaction properties, are summarized in Ling et al. (2000). The configuration of the PWRI Wall is shown in Fig. 1(a). The wall was constructed on a concrete floor to a height of 6.0 m. The wall face consisted of 12 concrete blocks, each 50 cm high and 35 cm wide, except the top and bottom blocks that were 45 cm and 55 cm high, respectively. Six primary (3.5 m long) and five secondary (1.0 m long) geosynthetic layers were installed in the backfill and bolted to the concrete block. The tensile strain in the reinforcement (52 locations), horizontal displacement of the wall face (11 locations), lateral force acting at the facing blocks (11 locations), and vertical stress along the base of the backfill (6 locations) were measured during construction.

**Dynamic Centrifuge Models**

A total of five dynamic centrifuge tests of geosynthetic-reinforced soil retaining walls were conducted using the facilities available at the Tokyo Institute of Technology (Takahashi et al. 1999; Takemura and Takahashi 2003). The models were 15 cm high and represented a prototype wall of height  $H = 7.5$  m under 50-g acceleration. The model wall was 21.5 cm long and had a 5 cm deep foundation [Fig. 1(b)]. The wall model was constructed in an aluminum container having inner dimensions of 45 cm (length) x 15 cm (width) x 25 cm (height). The side walls of the container were detachable. Rubber forms were used at the two ends of the model as boundary wave absorbers. Note that the curvature of the wall crest surface was introduced to accommodate the centrifugal acceleration field that varied across the length of model due to the inflight orientation of the centrifuge platform and container. Geosynthetic reinforcement of different lengths (0.6H, 0.8H and 1.0H) and vertical spacings (0.1H and 0.2H) were used. Table 1 summarizes the reinforcement layouts for the five tests.

The construction sequence of the reinforced soil wall, such as the placement of backfill, geogrid, wall facing, and compaction, was not modeled in flight. In fact, such a modeling technique was

**Table 2.** Parameters for Sands

Parameters		Public Works Research Institute Wall	
		sand	Inagi sand
$\phi_{p0}$ (°)	Peak value of the angle of internal friction at atmospheric pressure	39.4	33.0
$\Delta\phi$ (°)	Change of angle of internal friction with ten-fold increase in pressure	0.5	0
$M_g$	Slope of the critical state line in $p'-q$ plane	1.4	1.32
$M_f$	Slope of failure line in $p'-q$ plane	0.645	0.4
$G_0/p_a$	Normalized elastic modulus	500.0	800.0
$K_0/p_a$	Normalized bulk modulus	550.0	700.0
$k_s$	Parameter related to plastic coefficient	0.01	0.07
$\beta_{10}$	Parameter related to plastic coefficient	3.1	1.0
$\beta_0$	Parameter related to plastic coefficient	20.0	10.0
$\alpha$	Parameter related to soil dilatancy	0.47	0.25
$H_0/p_a$	Normalized plastic modulus number	500.0	190.0
$H_{u0}/p_a$	Normalized unloading plastic modulus number	—	800.
$r$	Coefficient related to stress memory factor	—	3.2
$r_u$	Exponent related to unloading plastic modulus	—	0.0
$r_d$	Parameter related to densification in unloading plastic modulus	—	350.0

found reasonable for earthquake loading where the dynamic effects are more significant than the static effects. The wall model was prepared under 1  $g$  conditions at an upside-down position by first laying down the wooden template in order to produce a curved backfill that met the orientation of the box in the centrifuge. The moist sand with the geogrids and accelerometers were introduced into the box and compacted statically in layers to the required density using a bellofram cylinder. The geogrid layers were attached to the aluminum facing panels of thickness 2 mm. The plates were hinged. At the end of construction, the bottom platen of the box was installed and the container was reversed to the upright position. The top plate was then removed and the displacement transducers were installed in front of the facing and along the wall crest.

The types and locations of the various instrumentations in the centrifuge models are shown in Fig. 1(b). A limited number of accelerometers, displacement transducers, and strain gauges were used because the small size of the model did not allow for intensive instrumentation compared to a full-scale model. In Tests 1–3, five accelerometers were used: Two were in the unreinforced backfill (A3,A7) and reinforced soil zone (A4,A8), respectively, and one measured the acceleration in the foundation soil (A9). In Tests 4 and 5, three accelerometers were used in the unreinforced (A1,A5,A7) and reinforced (A2,A6,A8) soil zones, respectively. In addition, the horizontal displacements of the wall facing were measured using two laser displacement transducers (D1, D2) and the settlement of the wall crest was measured at two locations using linear variable displacement transducers (S1,S2). Three geogrid layers were instrumented with strain gauges in each test. Four strain gauges for each layer were used in Tests 1 and 2, whereas three strain gauges were used in Test 3 (layers 1,3,5 from the bottom) and Tests 4 and 5 (layers 3,6,9 from the bottom). The first strain gauge was located 15 mm from the back of the panel, and the other gauges were 30 mm apart. However, as discussed later in the results, these strain gauges could not measure accurately the strain of the reinforcement because the epoxy used was stiffer than the reinforcement.

The container with the model wall was mounted to the shaking table in the centrifuge. After bringing the centrifuge to 50 $g$  acceleration, shaking was initiated using sinusoidal wave of 100 Hz (prototype frequency of 2 Hz). The input waves were of prototype

accelerations 0.2 $g$  having 20 cycles of shaking (0.25 or 12.5 s in prototype).

## Material Models

### Backfill Soils

The backfill soil used in PWRI Wall was a silty sand ( $D_{50} = 0.42$  mm,  $\gamma = 16.0$  kN/m<sup>3</sup>,  $C_u = 4.6$ ). In the dynamic centrifuge tests, Inagi sand ( $D_{50} = 0.4$  mm,  $\gamma = 17.8$  kN/m<sup>3</sup>,  $C_u = 2.3$ ) was used in the backfill and foundation. A generalized plasticity soil model (Ling and Liu 2003; Liu and Ling 2003) was used to express the soil behavior. The model used was an improvement over the Pastor–Zienkiewicz–Chan model (Pastor et al. 1990), which was developed specifically for simulating the behavior of sands under earthquake loading. It does not require a prescribed yield surface but uses loading direction vectors for determining the plastic strain increments. Upon modifications, the pressure-level dependency of the stiffness, dilatancy, and strength were considered. The model also considered improvements in simulating cyclic hardening behavior of sand. The model has been validated against the laboratory test results of several types of sand having different relative densities and under drained and undrained conditions (Ling and Liu 2003). The main details of the formulation of the model are summarized in the Appendix.

The generalized plasticity model requires 15 parameters for simulating cyclic loading, whereas 11 of these parameters can be obtained from static tests. The calibration followed the procedures outlined in Ling and Liu (2003). For the PWRI wall, three drained triaxial compression tests ( $\sigma_3 = 25$  kPa, 50 kPa, and 100 kPa) were used to obtain the 11 parameters related to monotonic loading. For the Inagi sand used in the centrifuge tests, two drained triaxial tests ( $\sigma_3 = 100$  kPa and 300 kPa) and a strain-control cyclic triaxial test ( $\sigma_3 = 100$  kPa, stress amplitude =  $-50$ – $85$  kPa) were used to calibrate the model. Table 2 summarizes the parameters and respective values for the two types of sand. Figs. 2(a)–2(c) show the comparison between the experimental and simulated results under static and cyclic loadings. The model was able to simulate the pressure-dependent stress–strain–dilatancy behavior satisfactorily.

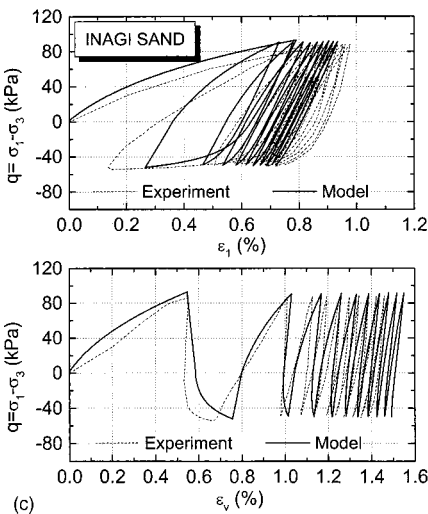
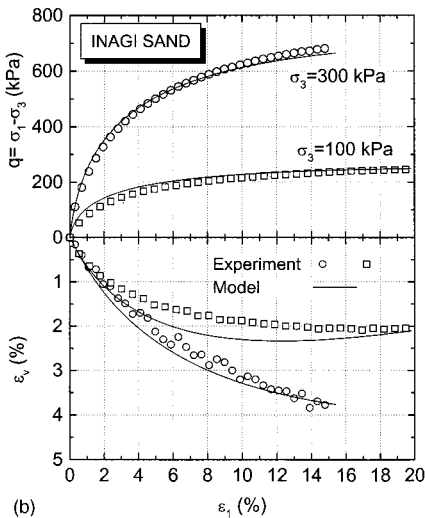
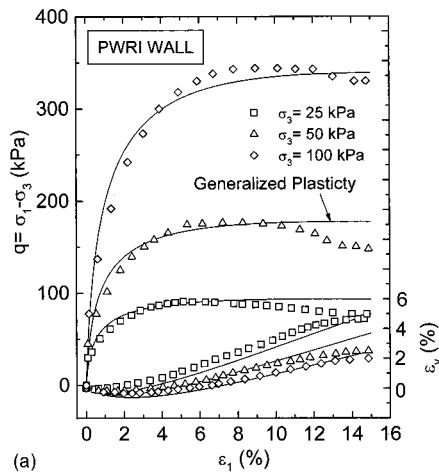


**Fig. 2.** Comparison between experimental and simulated soil triaxial test results: (a) Public Works Research Institute Wall—static, (b) Inagi sand—static, and (c) Inagi sand—cyclic

### Reinforcements

The PWRI Wall was reinforced with a high-density polyethylene (HDPE) uniaxial geogrid. The aperture size was 14.5 cm (machine direction) by 1.7 cm (cross-machine direction). The mass was 0.51 kg/m<sup>2</sup> and the tensile strength was 54 kN/m, which was

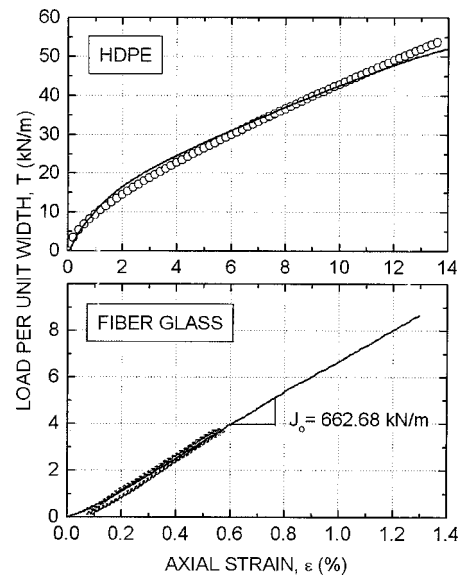


**Fig. 3.** Load–strain relationships of reinforcement: (a) High-density polyethylene geogrid and (b) fiber–glass screening

attained at an axial strain of 15%. A glass–fiber screening was used as geogrid in the centrifuge. Its aperture, thickness, and mass were 2.0 mm×1.5 mm, 0.2 mm, and 0.01 kg/m<sup>2</sup>, respectively (for 50g centrifuge, the lineal dimension has to be increased by 50 times). The tensile strength of this model geogrid was 8.64 kN/m and the rupture strain was 1.3%.

Ling et al. (2001b) formulated a bounding surface model to simulate the uniaxial cyclic behavior of geogrids. A total of nine parameters are required for cyclic loading, whereas in the case of monotonic loading, it is reduced to five parameters ( $Je$ ,  $A$ ,  $J_{p+}^o$ ,  $h_o^L$ , and  $h_k^L$ , where  $Je$  is the elastic stiffness,  $A$  and  $J_{p+}^o$  are used to define the bounding line, and  $h_o^L$  and  $h_k^L$  are for the hardening parameters during loading). Fig. 3 shows the tensile tests for the HDPE (strain rate of 10% per minute) and glass–fiber reinforcement (strain rate of 2.3% per minute) together with the results of simulation. The parameters used in simulating the monotonic test of HDPE are summarized in Table 3. Note that the glass–fiber reinforcement exhibited linear elastic behavior with negligible hysteresis for ten cycles of loadings [Fig. 3(b)], thus the load–strain relationship is defined by the elastic stiffness  $Je$ .

### Concrete Blocks, Interfaces, and Other Materials

The PWRI wall was constructed on a concrete foundation, which is assumed linear elastic. The concrete blocks were also assumed linear elastic with typical properties:  $E = 2.0 \times 10^6$  kPa,  $\nu = 0.17$ ,

**Table 3.** Parameters of Bounding Surface Model of Geogrid: Monotonic Loading (unit: kN/m)

Parameters	High-density polyethylene	Glass fiber
Elastic stiffness, $Je$	2,500.0	662.7
Bounding line parameters		
$A$	28.5	—
$J_{p+}^o$	281.0	—
Hardening parameters		
$h_o^L$	150.0	—
$h_k^L$	900.0	—

$\gamma=23 \text{ kN/m}^3$ . The block–block and soil–block interactions were studied using large-scale direct shear tests, from which the interface friction angles were obtained as  $\delta=19.6^\circ$  and  $16.5^\circ$ , respectively. Direct shear tests were also conducted to determine the angle of friction between the glass–fiber screening and Inagi sand. The interface friction angle was obtained as  $\delta=33.43^\circ$ , which was lower than the direct shear angle of friction of Inagi sand ( $38.8^\circ$ ).

The interface between the geogrid and sand was modeled for several cases of analysis. Thin layer elements having an elastic perfectly plastic sliding behavior were used. The elastic properties of the interface were  $E=5,000 \text{ kPa}$  and  $\nu=0$ . Since the geogrid layers were bolted to the blocks, the connection strength was assumed to be the failure strength of the geogrid and simulated using an elastic perfectly plastic interface model. The angle of friction between the soil and geogrid was larger than that of the block–block, block–geogrid, and block–soil. The relative displacement should occur between these interfaces before an opportunity for pullout will occur between the soil and geogrid, thus the geogrid layers were assumed to be fully compatible with the soil deformation.

The rubber foam and aluminum panel in the centrifuge models were assumed to be linear elastic materials having elastic moduli  $E=3,000 \text{ kPa}$  and  $7.0 \times 10^7 \text{ kPa}$ , respectively. The joint between the aluminum plates was modeled by assigning a small elastic modulus  $E=10.0 \text{ kPa}$ . Poisson's ratios for the rubber, aluminum and panel joint were  $\nu=0.5$ ,  $0.3$ , and  $0.0$ , respectively.

### Finite Element Simulation

The finite element analyses for both PWRI and centrifuge walls were conducted under two-dimensional plane strain conditions using a modified version of Diana–Swandynne-II (Chan 1993; Zienkiewicz et al. 1998). In this study, the finite element algorithms were modified to also handle automated construction together with additional material and element models (Liu 2002). The finite element meshes for the centrifuge models were designed considering the different vertical reinforcement spacings and lengths used in each test. The soil consisted of eight-node quadrilateral elements and six-node triangular elements, both calculated using full integration technique (nine-point and six-point integrations, respectively). The geogrid layer was simulated using three-node one-dimensional elements. In both PWRI wall and centrifuge models, the base is assumed to be rough/rigidly connected and the two ends are smooth.

A total of 38 increments were used to simulate the construction of the PWRI wall. Altogether 6,804 nodes and 2,314 elements, which included 115 bar elements for the geogrid reinforcements, were used. A total of 1,739, 360, 37, and 63 elements were used for the soil, concrete foundation, blocks, and interfaces, respectively. The solution was obtained using a quasi-Newton–Raphson nonlinear iteration scheme. The stiffness matrix was updated every 10 steps and a total of 500 steps was used in each increment with a convergence tolerance of 0.003.

Fig. 4 shows the mesh used for centrifuge Test 3. A total of approximately 1,000 elements were used, and the number differed slightly in each analysis because of the total number of layers of reinforcement and interfaces. A gravity turn-on analysis was first performed to obtain the initial stress conditions for the walls. The stresses at each Gauss point were used as the initial values for subsequent dynamic analysis. A nonlinear elastic model, whose shear modulus is dependent on the square root of the mean effective stress, was used in computing the initial stresses. A Mohr–

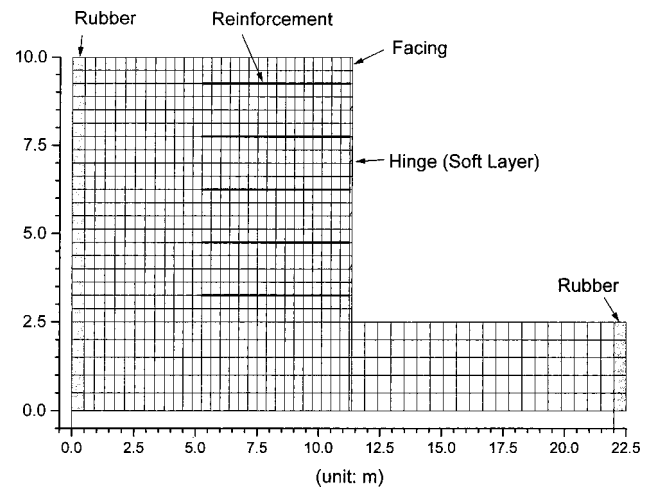


Fig. 4. Typical finite element mesh for centrifuge model (Test 3)

Coulomb failure criteria, with tension cutoff, was used to detect soil failure. The soil internal angle of friction and Poisson's ratio were assumed to be  $33^\circ$  and  $0.3$ , respectively.

The dynamic analysis was initiated using the input motion at the base of the mesh. In the dynamic analysis, the time integration was performed using the generalized Newmark method (Katona and Zienkiewicz 1985) with coefficients  $\beta_1=0.6$  and  $\beta_2=0.605$ . In addition to material damping that is simulated by the constitutive models, system viscous damping (Rayleigh damping) was considered in the analyses for the sand and interface (5%), rubber (10%), and aluminum (5%), where the values were determined based on the fundamental frequency of reinforced soil walls. No system damping was assigned to the geogrid. The analysis was iterated to convergence with a tolerance of 0.05 using the norm of relative displacements.

### Validation of Static Analysis: Public Works Research Institute Wall

The horizontal displacements of the wall, obtained from the analysis, are compared with the measured results for the different fill heights during the course of construction [Fig. 5(a)]. Note that each concrete block was represented by three elements and thus the results appeared clustered in sets of three. The measured and analyzed results agreed favorably for the construction height 4 m and above. It is of interest to mention that the results are close to those obtained from the nonlinear elastic analysis (Ling et al. 2000).

The lateral stress distributions behind the blocks at full height are shown in Fig. 5(b). The result at different elevations was obtained by averaging the values obtained from the 9 gauss points in the interface element. The results of analyses fluctuated along the wall height and this is typical for displacement-based finite element where stresses are determined as a secondary unknown from the displacements. The values differed within a soil element, whereas the values obtained from the integration points in the soil element located closest to the block are close to the average value of the interface elements. The distributions obtained from the analysis are close to the measured values for the wall height 5 m and above.

The vertical stress distributions at the foundation are presented in Fig. 5(c). The measured and analyzed values gave similar

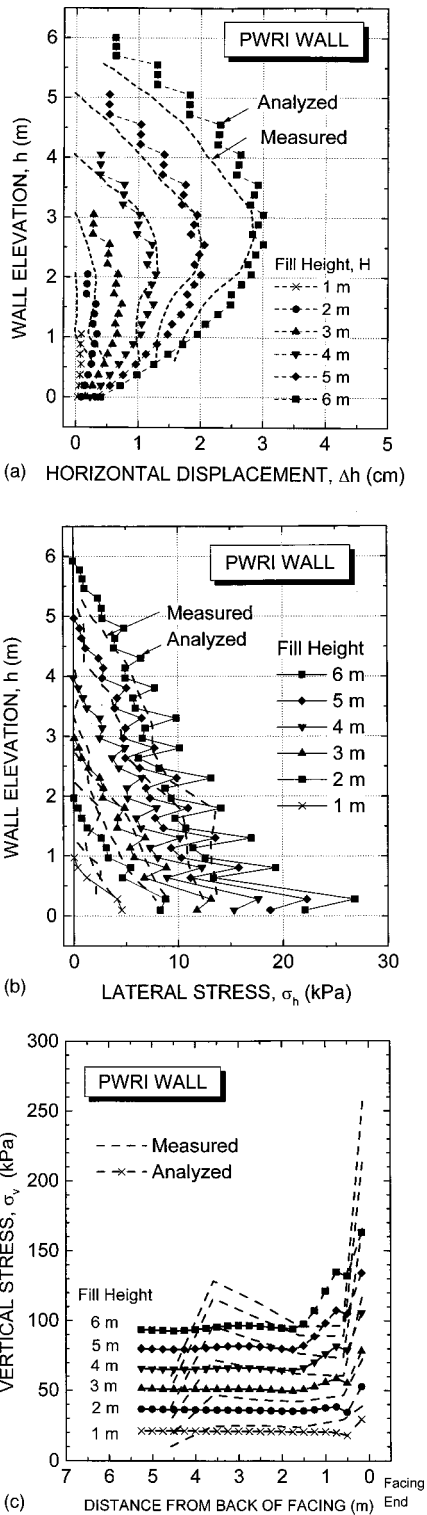


**Fig. 5.** Public Works Research Institute Wall results: (a) Facing horizontal displacement; (b) lateral earth pressure; and (c) vertical stress

trends where a larger vertical stress was obtained in the front end of the wall because of the unit weight and eccentricity of the concrete blocks. The measured results were larger than the finite element results. This could be due to the variation of soil unit weight with height by compaction as the height increased. However, the analysis assuming a linear elastic material for the con-

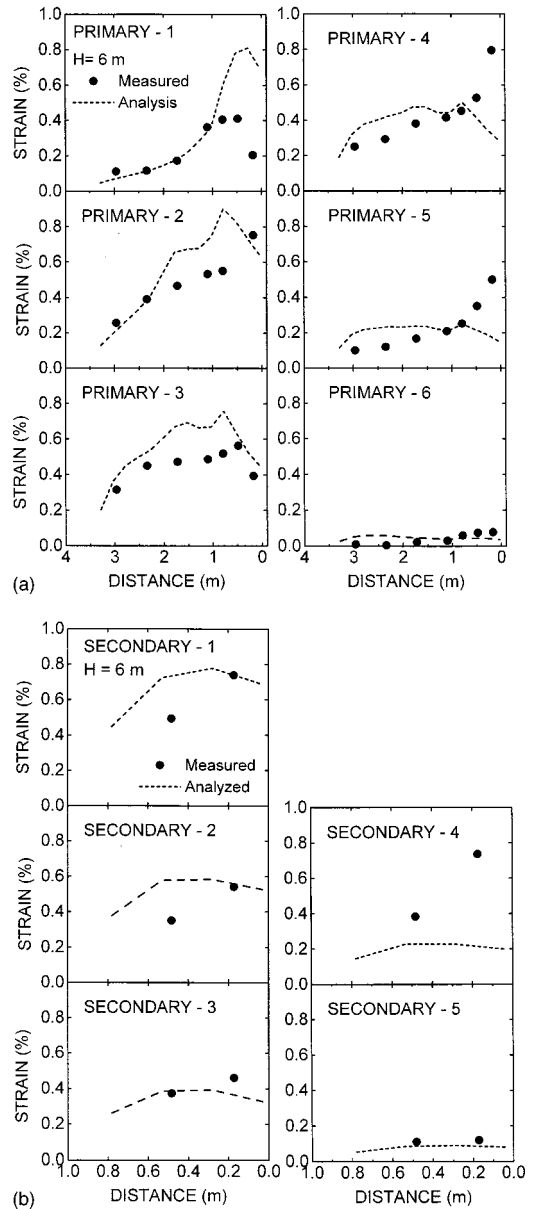


**Fig. 6.** Reinforcement strain distribution at full height: (a) Primary reinforcements and (b) secondary reinforcements

crete foundation, which is valid only for this test wall, cannot depict the nonuniform vertical stress distribution (Ling and Leshchinsky 2003).

The strain distributions in the six primary geogrid layers, with layer 1 located at the bottom and layer 6 at the top, are shown in Fig. 6(a) for the wall at its completed height. It is seen that the analyzed and measured results gave good agreement. The difference in results at the front end of the reinforcement layers could be attributed to the possible stress concentration due to relative settlement (overhanging) and creep in the geogrid that were not accounted for in the presented study. Note also that such a bolt and nut connection for the reinforcement is uncommon and limited to this particular test wall. The results at the back of the reinforcement were relatively well simulated. The results for the secondary reinforcement layers are given in Fig. 6(b).

#### Validation of Dynamic Analysis: Centrifuge Models

While the analysis was conducted using the dimensions of the centrifuge model, the results are presented for the prototype full-

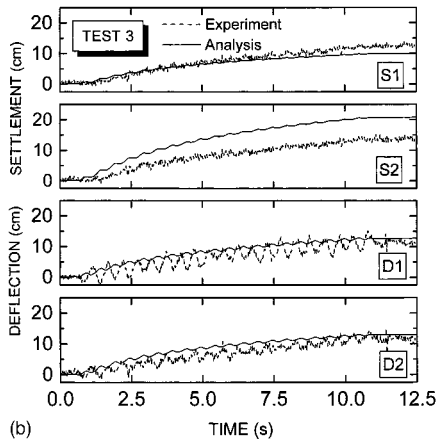
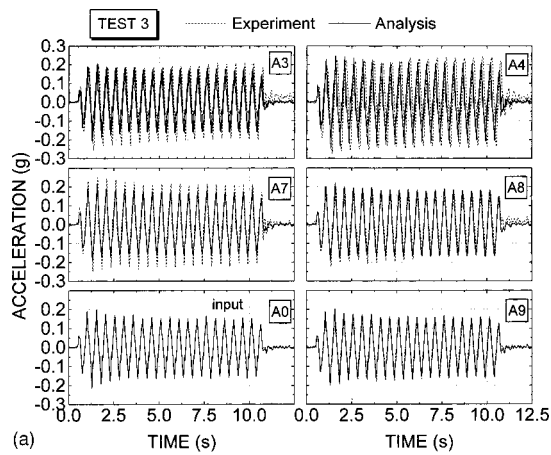


**Fig. 7.** Response of centrifuge Test 3: (a) Acceleration and (b) settlement and horizontal displacement

scale structures. The results obtained from the analysis are compared with the experimental results for the cyclic loading having an amplitude of  $0.2g$  subject to 12 s (20 cycles) shaking. Note that the interfaces between the soil–geogrid and soil–wall panel are not considered in these analyses. Liu (2002) has conducted additional studies that showed that the effects of modeling interfaces were very small for the five tests. Figs. 7(a and b) show typical results of acceleration response, wall face deflection, and settlement during duration of shaking in Test 3. The results for the four other tests, which are presented in Liu (2002), also gave good agreement.

The results showed that the acceleration amplified slightly with height for both reinforced and backfill zones. That is, the acceleration recorded at the wall surface is larger than the base input. This is summarized in Fig. 8 for the five tests where the amplification ratio, which is defined as the acceleration at the top of the wall to the input peak acceleration, was less than 1.5. However, in Tests 1 and 4, the measured value was slightly greater than 1.5. There was a little phase lag in acceleration recorded in the reinforced and unreinforced soil zones [see Fig. 7(a)].

The wall face displacement and crest settlement shown in Fig. 7(b) were accumulations of displacement over the period of 12 s shaking. Fig. 9 shows the comparison of wall face displacement at the end of shaking between the analyzed and measured values. There were, however, only two experimental values per wall. Except for Test 2, the experimental results are close to the results of

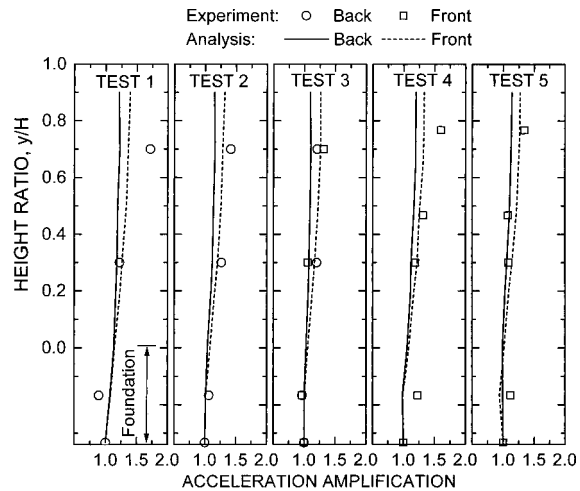


**Fig. 8.** Acceleration amplification in centrifuge tests

the analyses. Test 3 gave the largest horizontal deformation among the five tests, but it was less than 2% of the wall height.

The results of crest settlement are shown in Fig. 10. It is seen that the largest settlement occurred behind the reinforced zone, and was likely due to soil densification and also to the sliding out of the reinforced soil mass. Such results are seen only with the aid of numerical analysis because of the limited number of measurements in the centrifuge tests.

The maximum tensile strain in each geogrid layer was obtained and plotted in Fig. 11. The results showed that larger strains were mobilized in Tests 1, 2, and 3. Tests 4 and 5 gave a smaller maximum strain compared to the other tests because of smaller vertical reinforcement spacing. The measured results were smaller than computed due to the problem of strain gauge attachment. That is, the epoxy used in attaching the strain gauges was stiffer than the geogrid.

Based on the results of wall face deformations, Tests 3 and 5, which had the shortest reinforcement length, rendered the largest deformation. The strain in the reinforcement was also larger for shorter reinforcement length. Thus, an increased length of reinforcement minimizes lateral wall deformations and strains in the reinforcement layers. On the other hand, the acceleration ampli-

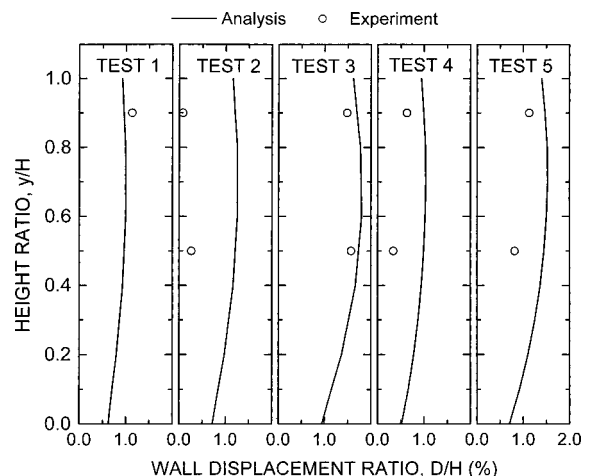


**Fig. 9.** Wall horizontal displacement in centrifuge tests

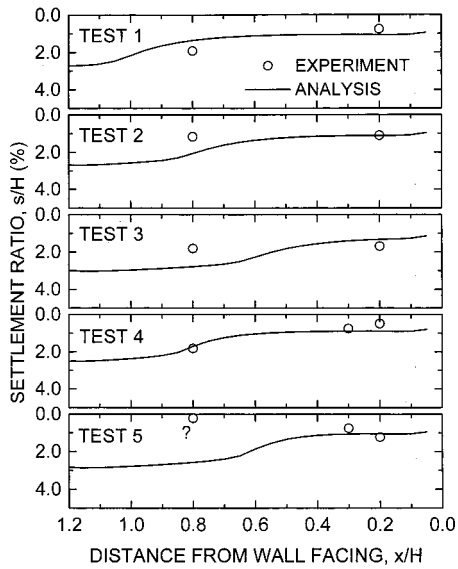


Fig. 10. Wall crest settlement in centrifuge tests

fication and crest settlement were not affected much by the length and spacing of the reinforcement.

### Summary and Conclusions

A finite element procedure, using a generalized plasticity model, was used to simulate the behavior of reinforced soil retaining walls. The behavior during construction and under sinusoidal excitation was simulated for two separate sets of tests. The study led to the following conclusions:

- The comparison of numerical and experimental results showed that the finite element procedure was able to simulate the construction behavior as well as dynamic behavior favorably. Thus, the generalized plasticity model for granular soil and the geosynthetic model were relevant for expressing the monotonic and cyclic behavior of soil and reinforcement, especially under cyclic loading.
- The results of analyses confirmed that the length and spacing of reinforcement played an important role in minimizing wall deformations and strains in the reinforcements.

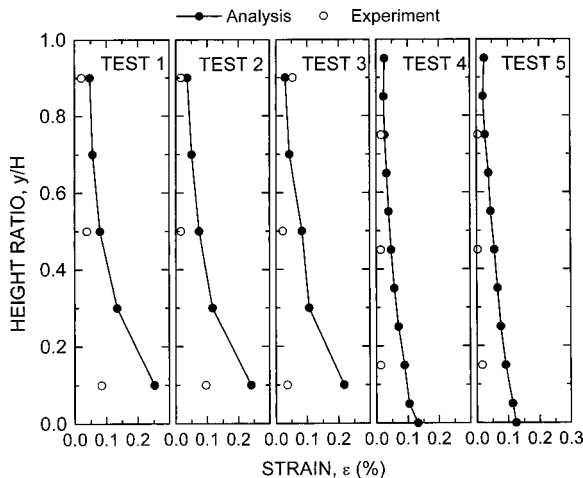


Fig. 11. Maximum tensile strain in reinforcement in centrifuge tests

- The amplification of acceleration seemed to be minimally affected by the reinforcement layout. It was around 1.5 for the walls of height 7.5 m.

The results presented in this study were limited to input motion consisting of a sinusoidal wave, which could be overidealized compared to real earthquakes. In addition, the validity between the centrifuge model and full-scale structures has to be confirmed. Large-scale shaking table tests are required for additional validation because centrifuge models cannot be extensively instrumented due to the size of model. Results of full-scale shaking table tests at a larger acceleration compared to the reported centrifuge tests are pursued in a separate publication (Ling et al. unpublished, 2003).

### Acknowledgments

This study was supported by the National Science Foundation through the Career Award CMS-0092739 granted to the first writer (H.I.L.), with Dr. Clifford J. Astill (currently Dr. Juan M. Pestana) as the Program Director. The centrifuge test program was a collaborative study with Japan and was supported by the NSF International Program INT-9996230 with Dr. Larry H. Weber as the Program Director. The Japanese counterpart at the Tokyo Institute of Technology (TIT) was supported by the Japan Society for Promotion of Science. Mr. Hijiri Hashimoto of PWRI, and Professor Jiro Takemura and Dr. Akihiro Takahashi of TIT provided the experimental results.

### Appendix

#### Generalized Plasticity Model

The formulation of generalized plasticity model with special accounts for the pressure level dependency and cyclic hardening are given below (after Ling and Liu 2003):

- Shear and bulk moduli:

$$G = G_o \bar{p}^{0.5} \quad (1)$$

$$K = K_o \bar{p}^{0.5} \quad (2)$$

where  $G$ ,  $K$ ,  $G_o$ ,  $K_o$ , and  $\bar{p}$  = shear modulus, bulk modulus, shear modulus number, bulk modulus number, and normalized mean stress (normalized by atmospheric pressure), respectively.

- Stress–dilatancy relationship:

$$d_g = (1 + \alpha)(M_g - \eta) \quad (3)$$

where  $d_g$  and  $\eta = q/p'$  = dilatancy and stress ratio;  $M_g$  = slope of the critical state line; and  $\alpha$  = constant.

The direction of plastic flow is determined by the following relationships:

$$d_f = (1 + \alpha)(M_f - \eta) \quad (4)$$

The plastic moduli for loading, unloading, and reloading are expressed through the following functions:

$$H_L = H_o \bar{p}^{0.5} H_f (H_v + H_s) \quad (5)$$

$$H_R = H_L \cdot H_{DM} H_{den} \quad (6)$$

$$H_U = H_{uo} \bar{p}^{0.5} \left( \frac{M_g}{\eta} \right)^{r_u} H_{den}; \quad \left| \frac{M_g}{\eta} \right| > 1 \quad (7a)$$

$$= H_{uo} \bar{p}^{0.5} H_{den}; \quad \left| \frac{M_g}{\eta} \right| \leq 1 \quad (7b)$$

where

$$H_f = \left(1 - \frac{\eta}{\eta_f}\right)^4 \quad (8)$$

$$H_v = 1 - \frac{\eta}{M_g} \quad (9)$$

$$H_s = \beta_1 e^{\exp\{k_s(p-1)/\beta_o \xi\}} \quad (10a)$$

$$\beta_1 = \beta_{10} \frac{\eta_p/M_g - 1}{\eta_{p0}/M_g - 1} \quad (10b)$$

$$H_{den} = \exp(-r_d \epsilon_{v0}^p) \quad (11)$$

where  $\xi$  and  $\epsilon_{v0}^p$  = deviatoric and volumetric plastic strains;  $\eta_f$ ,  $\eta_p$ , and  $\eta_{p0}$  indicate the stress ratios at failure, at peak strength and at reference stress level and a constant  $r$  is used in the memory state function  $H_{DM}$

$$\phi = \phi_0 \Delta \phi \log_{10} \bar{p}_a \quad (12)$$

where  $\phi_0$  = peak value of the angle of internal friction at atmospheric pressure and  $\Delta \phi$  = change of angle for a tenfold increase in pressure.

### Bounding Surface Model for Geosynthetic (Ling et al. 2001b)

Total stiffness

$$J_T = \frac{J_p J_e}{J_p + J_e} \quad (13)$$

Bounding line for monotonic loading

$$T_+ = A + J_{p+}^o \epsilon_p \quad (14)$$

Hardening parameters for monotonic loading

$$h^L = h_o^L + h_k^L \sqrt{\epsilon_p} \quad (15)$$

### Notation

The following symbols are used in this paper:

- $A$  = intercept of bounding line in geosynthetic model;
- $C_u$  = coefficient of uniformity;
- $D_{50}$  = mean grain diameter;
- $d_f, d_g$  = parameters related to loading direction vector, dilatancy;
- $E$  = Young's modulus;
- $G, G_0$  = elastic shear modulus, shear modulus number;
- $H_{DM}$  = stress memory factor in reloading modulus;
- $H_{den}$  = densification coefficient in unloading plastic modulus;
- $H_f, H_v, H_s$  = plastic coefficients;
- $H_L, H_R, H_U$  = loading, reloading, unloading plastic modulus;
- $H_0, H_{u0}$  = plastic modulus number, unloading plastic modulus number;
- $h_o^L, h_k^L$  = hardening parameters during loading in geosynthetic model;
- $J_e$  = elastic stiffness of geosynthetic;
- $J_{p+}^o$  = slope of bounding line in geosynthetic model;
- $K, K_0$  = bulk modulus, bulk modulus number;

- $k_s$  = parameter related to plastic coefficient  $H_s$ ;
- $M_f$  = slope of failure line in  $p'-q$  plane;
- $M_g$  = slope of the critical state line in  $p'-q$  plane;
- $p'$  = mean effective stress;
- $p_a$  = atmospheric pressure;
- $q$  = deviatoric stress;
- $r$  = coefficient related to  $H_{DM}$ ;
- $r_d, r_u$  = parameter and exponent related to  $H_{den}$  and  $H_u$ ;
- $\alpha$  = parameter related to soil dilatancy;
- $\beta_0, \beta_1, \beta_{10}$  = parameters related to plastic coefficient  $H_s$ ;
- $\gamma$  = unit weight;
- $\delta$  = interface friction angle;
- $\epsilon_{v0}^p$  = plastic volumetric strain at the instant of unloading or reloading;
- $\eta, \eta_f$  = stress ratio  $q/p'$ , stress ratio at failure;
- $\eta_p, \eta_{p0}$  = peak value of stress ratio, peak value of stress ratio at reference stress;
- $\nu$  = Poisson's ratio;
- $\xi$  = accumulative plastic deviatoric strain.
- $\sigma_1, \sigma_3$  = major and minor principal stresses; and
- $\phi, \phi_0, \Delta \phi$  = angle of internal friction, peak value of the angle of internal friction, change of angle with ten-fold increase in pressure.

### References

- Bathurst, R. J., Walters, D. L., Hatami, K., and Allen, T. M. (2001). "Full-scale performance testing and numerical modeling of reinforced soil retaining walls." *IS Kyushu preprint*, 3–28.
- Bolton, M. D., Choudhury, S. P., and Pang, P. L. R. (1979). "Reinforced earth walls: A centrifugal model study." *Proc., ASCE Symp. on Earth Reinforcement*, ASCE, New York, 252–281.
- Cai, Z., and Bathurst, R. J. (1995). "Seismic response analysis of geosynthetic reinforced soil segmental retaining walls by finite element method." *Comput. Geotech.*, 17, 523–546.
- Chan, A. H. C. (1993). *User Manual for Diana-Swandyne-II*, Department of Civil Engineering, Glasgow Univ., U.K.
- Collin, J. G. (1986). "Earth Wall design." PhD thesis, Univ. of California, Berkeley, Calif.
- Helwany, S. M. B., Budhu, M., and McCallen, D. (2001). "Seismic analysis of segmental retaining walls. I: Model verification." *J. Geotech. Geoenviron. Eng.*, 127(9), 741–749.
- Jaber, M. B., Mitchell, J. K., Christopher, B. R., and Kutter, B. L. (1990). "Large centrifuge modeling of full scale reinforced soil walls." *Design and Performance of Earth Retaining Structures, GSP 25*, ASCE New York, 379–393.
- Kaliakin, V. N., and Xi, F. (1992). "Modeling of interfaces in finite element analyses of geosynthetically reinforced walls." *Earth reinforcement practice*, H. Ochiai et al., eds., Balkema, Rotterdam, The Netherlands, 351–356.
- Kapurapu, R., and Bathurst, R. J. (1995). "Behavior of geosynthetic reinforced soil retaining walls using the finite element methods." *Comput. Geotech.*, 17, 279–299.
- Katona, M. G., and Zienkiewicz, O. C. (1985). "A unified set of single step algorithms. III: The beta- $m$  method, a generalization of the Newmark scheme." *Int. J. Numer. Methods Eng.*, 21(9), 1345–1359.
- Koseki, J. et al. (2003). "Model tests on seismic stability of several types of soil retaining wall." *Reinforced soil engineering: Advances in research and practice*, Ling, H. I., Leshchinsky, D. and F., Tatsuoka, eds., Marcel Dekker, New York, 317–358.
- Kutter, B. L., Casey, J. A., and Romstad, K. M. (1990). "Centrifuge modeling and field observations of dynamic behavior of reinforced

- soil and concrete cantilever retaining walls." *Proc., 4th U.S. National Conf. on Earthquake Engineering*, 663–672.
- Ling, H. I., Tatsuoka, F., and Tateyama, M. (1995). "Simulating performance of GRS-RW by finite-element procedure." *J. Geotech. Eng.*, 121(4), 330–340.
- Ling, H. I., Cardany, C. P., Sun, L.-X., and Hashimoto, H. (2000). "Finite element study of a geosynthetic-reinforced soil retaining wall with concrete-block facing." *Geosynthet.*, 7(3), 163–188.
- Ling, H. I., Leshchinsky, D., and Chou, N. N. S. (2001a). "Postearthquake investigation on several geosynthetic-reinforced soil retaining walls and slopes during 1999 Ji-Ji Earthquake of Taiwan." *Soil Dyn. Earthquake Eng.*, 21(4), 297–313.
- Ling, H. I., Liu, H., Mohri, Y., and Kawabata, T. (2001b). "A bounding surface model for geosynthetic reinforcements." *J. Eng. Mech.*, 127(9), 963–967.
- Ling, H. I., and Leshchinsky, D. (2003). "Finite element parameter studies of the behavior of segmental block reinforced soil retaining walls." *Geosynthet. Int.*, 10(3), 77–94.
- Ling, H. I., and Liu, H. (2003). "Pressure-level dependency and densification behavior of sand through generalized plasticity model." *J. Eng. Mech.*, 129(8), 851–860.
- Liu, H. (2002). "Finite element simulation of the response of geosynthetic-reinforced soil walls." PhD thesis, Columbia Univ., New York.
- Liu, H., and Ling, H. I. (2003). "A sand model based on generalized plasticity." *Constitutive modeling of geomaterials: Selected contributions from Frank L. DiMaggio symposium*, H. I. Ling, A. Anandaraman, M. T. Manzari, V. N. Kaliakin, and A. Smyth, eds., CRC Press, Boca Raton, Fla., 40–46.
- Pastor, M., Zienkiewicz, O. C., and Chan, A. H. C. (1990). "Generalized plasticity and the modeling of soil behavior." *Int. J. Numer. Analyt. Meth. Geomech.*, 14, 151–190.
- Porbaha, A., and Goodings, D. J. (1996). "Centrifuge modeling of geotextile-reinforced cohesive soil retaining walls." *J. Geotech. Eng.*, 122(10), 840–848.
- Rowe, R. K., and Ho, S. K. (1997). "Continuous panel reinforced soil walls on rigid foundations." *Liq. Cryst. Ordered Fluids*, 123(10), 912–920.
- Sakaguchi, M. (1996). "A study of the seismic behavior of geosynthetic reinforced walls in Japan." *Geosynthet.*, 3(1), 13–30.
- Segrestin, P., and Bastick, M. J. (1988). "Seismic design of reinforced earth retaining walls—The contribution of finite element analysis." *Theory and practice of earth reinforcement*, H. Ochiai et al., eds., Balkema, Rotterdam, The Netherlands, 577–582.
- Tajiri, N., Sasaki, H., Nishimura, J., Ochiai, Y., and Dobashi, K. (1996). "Full-scale failure experiments of geotextile-reinforced soil walls with different facings." *Earth reinforcement*, H. Ochiai et al., eds., Balkema, Rotterdam, The Netherlands, 525–530.
- Takahashi, A., Takemura, J., and Izawa, J. (1999). "Dynamic behavior of vertical geogrid-reinforced soil during earthquake." *Proc., Int. Symp. on Slope Stability Engineering*, N. Yagi, T. Yomagami, and J.-C. Jiang, eds., Balkema, Rotterdam, The Netherlands, Vol. 2, 991–996.
- Takemura, J., and Takahashi, A. (2003). "Centrifuge modeling of seismic performance of reinforced earth structure." *Reinforced soil engineering: Advances in research and practice*, H. I. Ling, D. Leshchinsky, and F. Tatsuoka, eds., Marcel Dekker, New York, 417–442.
- Tatsuoka, F., Koseki, J., Tateyama, M., Munaf, Y., and Horii, K. (1998). "Seismic stability against high seismic loads of geosynthetic-reinforced soil retaining structures." *6th Int. Conf. on Geosynthetics*, Atlanta, 103–142.
- Yogendrakumar, M., Bathurst, R. J., and Finn, W. D. L. (1992). "Dynamic response analysis of reinforced-soil retaining wall." *J. Geotech. Eng.*, 118(8), 1158–1167.
- Zienkiewicz, O. C., Chan, A. H. C., Pastor, M., Schrefler, B. A., and Shiomi, T. (1998). *Computational geomechanics with special reference to earthquake engineering*, Wiley, Chichester, England.
- Zornberg, J. G., Sitar, N., and Mitchell, J. K. (1998). "Performance of geosynthetic reinforced slopes at failure." *Liq. Cryst. Ordered Fluids*, 124(8), 670–683.